Microelectronic Engineering 157 (2016) 35–41

Contents lists available at ScienceDirect

Microelectronic Engineering

journal homepage: www.elsevier.com/locate/mee

Electrical transport mechanisms and photovoltaic characteristics of Au/neutral red/p-Si/Al heterojunction solar cell

H.M. Zeyada [a], M.M. Makhlouf [b,c,*], M.M. El-Shabaan [a], M.H. Zeyada [d]

[a] Department of Physics, Faculty of Science, University of Damietta, 34517 New Damietta, Egypt
[b] Department of Physics, Faculty of Applied Medical Sciences at Turabah, University of Taif, 21995, Saudi Arabia
[c] Department of Physics, Damietta Cancer Institute, Damietta, Egypt
[d] Department of Computer Engineering and Systems, Faculty of Engineering, University of Mansoura, 35516, Egypt

ARTICLE INFO

Article history:
Received 14 October 2015
Received in revised form 3 February 2016
Accepted 4 February 2016
Available online 11 February 2016

Keywords:
Neutral red
Thin films
Conduction mechanisms
Photovoltaic properties
Heterojunction solar cell

ABSTRACT

Uniform thin films of neutral red, NR, have been successfully prepared by thermal evaporation technique. X-ray diffraction patterns showed that the structure of NR film consists of nanocrystallites dispersed in amorphous matrix. Increasing annealing temperature influences crystallite size and quantity of amorphous phase. The high absorption of NR films in visible region of spectra supports the application of NR film as an absorber in photovoltaic devices. Hybrid organic–inorganic heterojunction solar cell, Au/NR/p-Si/Al, was fabricated. The current–voltage characteristics of the heterojunction diode have been studied in the temperature range of 300–355 K and in the voltage range (−2 to 2 V). The device showed a series resistance of 2.64 kΩ, shunt resistance of 237 kΩ, rectification ratio of 106 at ±1 V and ideality factor of 1.8 at room temperature. It was found that the conduction mechanisms of the diode are controlled by the thermionic emission at forward voltage bias ≤0.2 V and space charge limited current (SCLC) conduction in the voltage range $0.2 < V \leq 2$ V. The capacitance–voltage characteristics of the NR/p-Si device were studied at room temperature in dark condition. Energy band diagram for NR/p-Si device was constructed. The device under illumination with light of intensity 20 mW/cm^2 gives values of photovoltaic parameters as: open circuit voltage (V_{oc}), short circuit current (I_{sc}), fill factor (*FF*) and power conversion efficiency (η) are 0.46 V, 1.78 mA, 0.29 and 2.37%, respectively.

1. Introduction

In recent years, the photovoltaic technology has a growing research interest due to the increasing demand for renewable and clean energy. Dyes are promising organic materials for applications in liquid crystal displays [1], photovoltaic cells [2], sensors [3] and it is used in dye sensitized solar cells (DSSCs) [4,5]. The DSSC is distinguished in that it resembles natural photosynthesis in two respects: it uses an organic dye to absorb light and produces a flow of electrons and multiple layers to enhance both the absorption and efficiency of the DSSC. Investigations of organic–inorganic heterojunction devices attract some interest due to both the unusual nature of these contacts as well as to the potential new devices that can be applied. Recently, different organic–inorganic heterojunctions such as pyronine-B /Si [6], b-carotene/Si [7], chitin/n-Si [8], and MEH-PPV/p-Si [9] have been fabricated and then the electronic parameters have been measured in each fabricated junction.

Organic thin films have several clear advantages over inorganic thin films such as large-area coverage, mechanical flexibility, low-temperature process capability, easy preparation and low cost. Neutral red, NR, is an organic dye belonging to the phenazine family that are mainly used as aromatic dyes [10]. NR was first prepared by Witt [11] via condensation of p-nitrosodimethylanaline and 2,4-daimino-toluene in aqueous medium and oxidization of the resulting toluylene blue by ferric chloride. NR, dye which is used in the present work has molecular formula $C_{24}H_{28}N_3Cl$. The structure skeleton of NR has an extended π-conjugation system due to the delocalization of electrons in the benzene, methyl and amine functional groups and that leading to a wide range of high optical absorption in visible spectrum. NR is thermochromic [1,12] and photochromic [1,13] materials. Influence of γ-ray irradiation on the spectral characteristics and absorption spectrum of NR thin films deposited by thermal evaporation technique have been studied [14]. The type of electron transition and energy band gap, optical constants, optical dispersion parameters and dielectric constants of NR thin films were also measured. All of these studies showed that NR compound has a high optical absorption in visible region of spectrum with onset band-gap of 1.75 eV that recommend them to be used in optoelectronic device fabrication [14]. The application of NR in solar cell fabrication process will be provided as thin film sandwich. The sandwich may be constructed in homo- or heterojunction configuration. Such homojunction devices have loss factors including; photo carrier generation is a function not only of bulk optical

* Corresponding author at: Department of Physics, Faculty of Applied Medical Sciences at Turabah, University of Taif, 21995, Saudi Arabia.
E-mail addresses: m_makhlof@hotmail.com, m.m.makhlouf@hotmail.com (M.M. Makhlouf).

http://dx.doi.org/10.1016/j.mee.2016.02.011
0167-9317/

absorption, but also of available mechanisms for exciton dissociation, non-irradiative recombination at the interfaces and non-geminate recombination at impurities. Single layer solar cells of this type deliver quantum efficiencies of less than 1% and power conversion efficiencies of less than 0.1% [15]. In heterojunction devices, the local electric fields are strong and may break up photo generated exciton provided that the differences in potential energy are larger than the exciton binding energy. The organic donor–acceptor interface separates exciton much more efficiently than the organic/metal interface; efficient photovoltaic devices may be made from heterojunction configuration.

To our knowledge, NR is one of the less reported dyes in literatures. The electrical properties of NR thin films have not been investigated yet. In the present work, the attention has been focused on fabricating a hybrid heterojunction solar cell of Au/NR/p-Si/Al and providing an investigation about its electronic transport mechanisms and photovoltaic properties.

2. Experimental details

A brownish-black powder of NR (IUPAC name: 3-Amino-7-dimethylamino-2-methylphenazine hydrochloride) was purchased from Sigma-Aldrich Co. (USA) and was used in as-received condition without any further purification.

NR thin films of thickness 407 nm were prepared by thermal evaporation technique. The high vacuum coating unit was used for this purpose. Initially, the pressure inside the vacuum work chamber was pumped down to 10^{-5} mbar. Evaporation of the NR material is carried out with quartz crucible heated by boat-shaped molybdenum heater while Au and Al electrodes were thermally evaporated by using basket-shaped tungsten filament. Rate of deposition and film thickness were controlled by using quartz crystal thickness monitor. The deposition rate was controlled at 2.5 Å/s.

The X-ray diffraction, XRD, patterns for NR as thin film were performed by a diffraction system utilizing CuK_α radiation (λ = 1.5418 Å). The X-ray tube current is 30 mA and the applied potential is 40 kV. Thin films of NR were annealed at different annealing temperatures in a tubular vacuum furnace with a soaking time of 1 h.

The hybrid Au/NR/p-Si/Al solar cell was fabricated by thermal evaporation of NR and Al electrodes on the surfaces of p-Si substrate. NR was deposited on polished surface of Si substrate and Al was thermally evaporated on rough surface of Si substrate. A mesh of Au electrode was thermally deposited on the surface of NR. The Si substrate is a p-type single crystal wafer with one polished face, the hole concentration of p-type Si single crystal wafer is 1.6×10^{23} m^{-3} and its thickness is 400 μm. First, the p-Si wafer was chemically cleaned and etched by PC4 solution (HF: HNO_3: CH_3COOH in ratio 1:3:1) for 10 s, then rinsed with deionized water and isopropyl alcohol and oven-dried. The hybrid junction of Au/NR/p-Si/Al solar cell was fabricated according to the following steps; the back contact electrode was made by depositing a relatively thick film of pure Al to the p-Si substrate. NR with thickness of 95 nm was deposited on the front surface of p-Si wafer. Then, a front of pure Au was evaporated on NR layer as a mesh grid electrode. The active area of the solar cell is 0.5 cm^2.

The electrical resistivity of NR films was measured by high impedance electrometer. The independent stabilized DC power supply of the electrometer was used as a power supply. All measurements were taken in dark at different temperatures in ambient atmosphere. The current–voltage, I–V, characteristics of the virgin heterojunction device were measured under dark and illumination conditions for different annealing temperatures. The incident power density of light illumination provided by tungsten filament lamp was 20 mW/cm^2. The intensity of the incident light was measured by using a digital lux-meter.

The UV–vis absorption spectra of NR thin film deposited onto optically flat fused quartz substrates were recorded by spectrophotometer. All these spectra were recorded at room temperature.

The capacitance of the NR/p-Si cell was measured at a high frequency of 1 MHz using a computerized meter in dark and at room temperature.

3. Results and discussion

3.1. X-ray diffraction patterns for NR

The X-ray diffraction, XRD, pattern for NR in powder form is given elsewhere [14]. Identification of XRD pattern of NR in powder form was performed by using [16,17] and it showed that it has a triclinic crystal system and space group p1 with lattice parameters: a = 10.27 Å, b = 14.77 Å, c = 16.45 Å, α = 72.67°, β = 111.61° and γ = 81.83°. The XRD pattern for pristine thin film of NR of thickness 407 nm is illustrated in Fig. 1; a single diffraction peak at ($2\theta = 25°$) corresponding to diffraction from ($1\ \bar{3}0$) superimposed on amorphous phase is observed.

The effect of annealing temperatures on the XRD patterns of the NR thin films with thickness 407 nm is shown also in Fig. 1. The assignment of diffraction peaks in Fig. 1 was obtained from XRD pattern of polycrystalline powder [14]. Annealing at 343 K did not affect the peak position of diffraction ($1\ \bar{3}0$) of pristine NR film and slightly increased its intensity. Annealing NR films at 443 K nucleates a new diffraction peak at ($2\theta = 31.75°$) corresponding to diffraction from (1 5 0) and a halo at 2θ angular range of 14–38°; this indicates partial transformation of nanocrystallite NR phase into amorphous one. Changes in the intensities of X-ray diffraction peaks may result from grain growth and large amounts of intrinsic stresses, the stresses resulting at the early stages of growth; the magnitude of these stresses depends upon both the film thickness and annealing temperatures.

The mean crystallite size, D, of the film was estimated by using the Scherrer expression [18]. The calculated crystallite size of nanocrystals in pristine film is 97 nm. In annealed NR film (343 K with a soaking time of 1 h); the sharp diffraction peak corresponds to reflection from ($1\ \bar{3}\ 0$) is retained and the amount of amorphous phase of NR is significantly decreased. The calculated crystallite size is 17 nm. Increasing annealing temperature to 443 K increases the amount of amorphous phase and a new diffraction peak appeared corresponding to diffraction from the (1 5 0). The determined crystallite size [18] for the annealed film at 443 K is 100 nm.

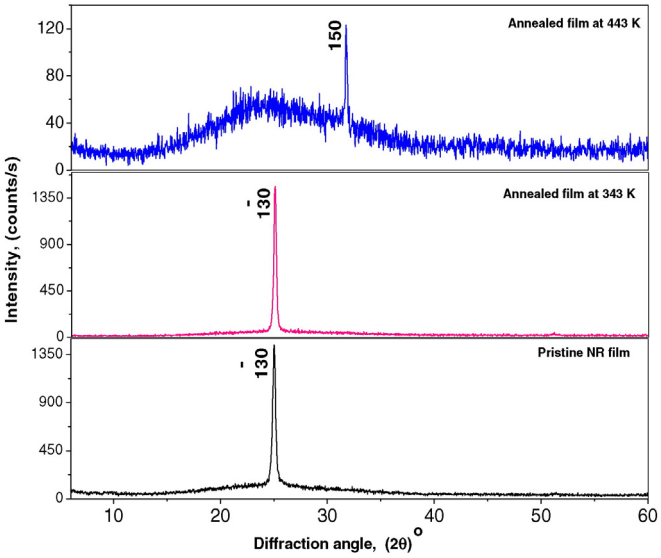

Fig. 1. XRD pattern for pristine and annealed NR films.

3.2. Absorption spectrum of NR thin film

Fig. 2 illustrates absorption spectra for the pristine and annealed NR thin films. There are two absorption bands in UV and visible regions of spectra whose peaks are at λ_{max} of 269 and 465 nm, respectively. These bands are attributed to electronic transitions either between n and π^* orbital or between π and π^* orbital depending on the position of absorption peak in the spectra. There is also a sharp absorption edge in wavelength range 534–680 nm. At 680 nm, absorption spectrum starts to decrease slowly with increasing wavelength and formed a tail which is a characteristic feature of existence of localized states in the band gap enriched with free carriers. The type of electronic transition for NR thin films is found to be indirect allowed transition, the onset and optical energy gaps for pristine film were calculated as 1.75 and 3.23 eV, respectively [14]. Annealing temperature decreases absorption all over the spectrum and reduces peaks intensity in UV and visible region of spectra. The decrease of absorption resulting from annealing NR film at 343 K is a result of decreasing crystallite size and the significant decrease of absorption resulting from annealing NR film at 442 K is attributed to the increase of volume fraction of amorphous phase in the matrix.

3.3. DC dark current–voltage characteristics

Fig. 3 illustrates the dark current–voltage (I–V) characteristics of Au/NR/p-Si/Al heterojunction solar cell measured at different temperatures ranging from 303 to 355 K in voltage range from −2 to 2 V. The results show typical diode behavior where at a certain applied voltage; the current increases with increasing temperature indicating a negative temperature coefficient for the resistivity [19]. The low and weak voltage dependence of the reverse bias current as well as the strong voltage dependence of the forward bias current are characteristic properties of strong rectification performance for the junction diode. The rectification ratio at room temperature has been estimated from Fig. 3 as 106 at ±1 V. The series resistance (material resistance and contact resistance in the junction) and the shunt resistance (the resistance due to the leakage current through the junction) are important parameters in determining cell performance [20]. Their values can be calculated from the slope of the linear part of the forward and reverse I–V curve at room temperature, respectively. The series, R_s, and the shunt, R_{sh}, resistances are determined at room temperature as 2.64 kΩ and 237 kΩ, respectively.

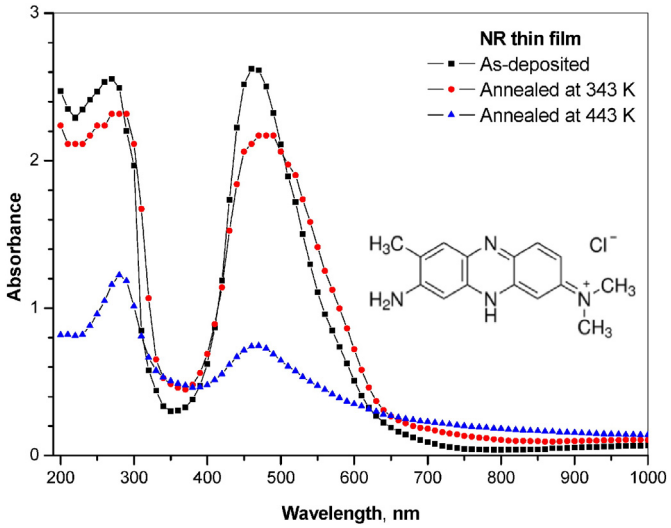

Fig. 2. Absorption spectra of NR thin films: (a) pristine and (b) annealed at 343 and 443 K.

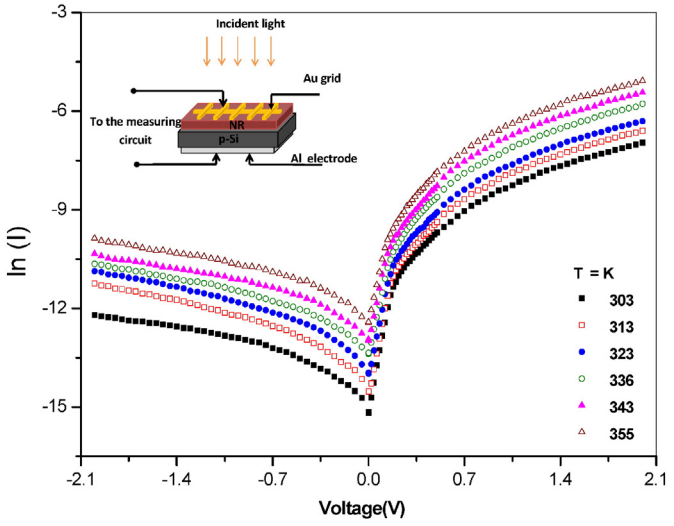

Fig. 3. Semi-logarithmic plot of dark I–V characteristics of Au/NR/p-Si/Al heterojunction solar cell at different temperatures for forward and the reverse bias. The inset shows schematic diagram showing the construction of Au/NR/p-Si/Al heterojunction solar cell.

Results of Fig. 3 shows that the current of the device obeys the standard diode expression given by [21]:

$$I = I_s \exp\left(\frac{eV - IR_s}{nk_BT} - 1\right)\left[1 - \exp\left(\frac{-e(V - IR_s)}{k_BT}\right)\right], \quad (1)$$

where I_s is the saturation current, e is electron charge, V is the applied voltage across the device, T is the absolute temperature and n is the ideality factor. According to that equation the ideality factor, n, is given by [21]:

$$n = \frac{e}{k_BT}\left(\frac{dV}{d\ln I}\right). \quad (2)$$

The ideality factor gives information about the recombination process, which takes place in the device and shape of the interfaces, i.e. the internal bulk morphology for organic devices [22]. The ideality factor is determined at different temperatures and it decreases with increasing the temperature from 1.80 to 1.66. The device was non-ideal in showing the value of $n > 1$; the deviation of n far from unity may be attributed to either recombination of electrons with holes in the depletion region, and/or the increase in the diffusion current due to increase in the applied potential [23]. The high values of the ideality factor in the prepared junctions may be attributed to factors such as interfacial layer thickness, leakage current, shunt and series resistances, or any other resistive loss [23,24]. The obtained value of n in our case is due to relative high values of R_s and R_{sh}. The decrease of ideality factor with temperature may be attributed to softening occurring in NR as a result of partial transformation of nanocrystallites NR phase to amorphous one at 443 K as shown previously in Fig. 1.

The information about the operating conduction mechanisms can be obtained from the I–V characteristics at different temperatures illustrated in Fig. 3. There are two distinct regions characterizing these curves and indicating that there are two different conduction mechanisms. The relationship between ln I and V in voltage range $0 < V < 0.2$ of Fig. 3 shows straight lines for different temperatures; this indicates that thermionic emission is the operating conduction mechanism in this potential range. The saturation current (I_s) in the thermionic emission model is expressed as [25]:

$$I_s = AA^{**}T^2 \exp\left(\frac{-e\phi_b}{k_BT}\right) \quad (3)$$

where A is the effective area of the device, A^{**} is the Richardson constant ($A^{**} = 32$ A/cm^2 K^2 for p-Si [25]) and φ_b is the effective barrier height at the p-NR/p-Si interface at zero bias potential. The saturation current was obtained at different temperatures from the intercept of the linear part in semi-logarithmic plot with the current axis at zero voltage (Fig. 3). A plot of ln (I_s/T^2) as a function of 1/T is demonstrated in Fig. 4. The effective barrier height φ_b at zero bias potential was calculated from the slope in Fig. 4 and it was found to be 0.45 eV.

In the potential region ($0.2 < V < 2$), other conduction mechanism seems to be dominant. It is observed that the current shows a power dependence of voltage ($I \propto V^m$) with slope of ln I − ln V of about ≈ 2 as seen from plot in Fig. 5; this power dependence suggests that the dark current is a space-charge-limited current (SCLC) dominated by a single trap level. According to Lampert theory, the relation for the current in this case is given by [26] as:

$$I_{SCLC} = \frac{9}{8}\varepsilon\mu A\theta\frac{V^2}{d^3} \quad (4)$$

where d is the thickness of the NR film, ε is the permittivity of NR, μ is the mobility of holes and θ is the trapping factor, which is defined by the ratio of the free charges to trapped charges and it is given by

$$\theta = \frac{N_v}{N_{t(s)}}\exp\left(\frac{-E_t}{k_B T}\right) \quad (5)$$

where N_v is the effective density of states in the valence band edge, and $N_{t(s)}$ is the total trap concentration at energy level E_t above the valence band edge. Substituting Eq. (5) in Eq. (4); it is evident that ln I versus inverse of temperature at constant applied potential should be straight lines as shown in Fig. 6. The slope and intercept with the ordinate axis are used for estimating the values of E_t and $N_{t(s)}$, respectively. The relative permittivity of the NR thin films $\varepsilon_r = 3.07$ [14], the permittivity of the free space is $\varepsilon_o = 8.85 \times 10^{-12}$ F m^{-1} then the permittivity of the NR was calculated as $\varepsilon = 2.7 \times 10^{-11}$ Fm^{-1} [10]. Assuming that the average mobility of carriers and the effective density of states in the valence band edge for phenazines are $\mu = 10^{-7}$ m^{2}V^{-1} s^{-1} and $N_v = 10^{27}$ m^{-3} V, respectively [14,27]. Substituting these values in Eqs.(4) and (5), the total trap concentration, $N_{t(s)}$, was estimated as 2.31×10^{25}, 7.1×10^{25} and 1.4×10^{26} m^{-3} at 0.5, 1 and 1.5 applied voltages, respectively. The single trap level, E_t was calculated as 0.341, 0.339 and 0.346 eV at 0.5, 1 and 1.5 applied voltages, respectively. By using the average value of the total trap concentration $N_{t(s)}$ (7.1×10^{25} m^{-3}) and

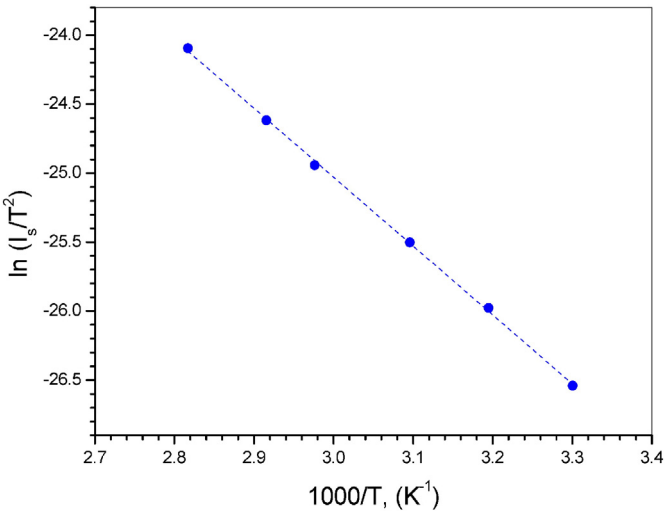

Fig. 4. Dependence of ln (I_s/T^2) on reciprocal temperature for Au/NR/p-Si/Al heterojunction diode at zero biasing.

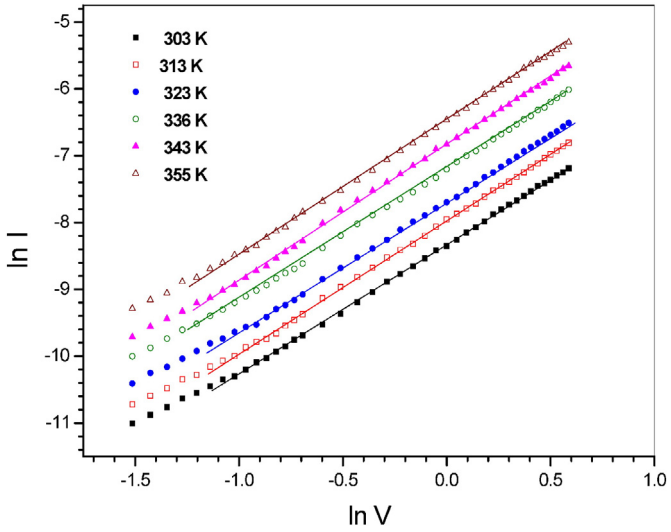

Fig. 5. Double-logarithmic plot of the forward bias (I–V) characteristic of Au/p-NR/p-Si/Al heterojunction cell in voltage range 0.2 < V < 2 at different temperatures.

the single traps level $E_t = 0.339$ eV the value of the trapping factor θ was calculated as 7.7×10^{-7}.

3.4. Capacitance–voltage characteristics of Au/NR/p-Si/Al heterojunction solar cell

The junction capacitance (C) of a diode as a function of the reverse bias voltage (V_r) is given by [19,28]:

$$C = \frac{C_o}{\left(1 + \frac{V_r}{V_b}\right)^g} \quad (6)$$

where C_o is the zero bias junction capacitance and g is a coefficient whose value depends on the nature of the junction, it takes the value of 1/2 and 1/3 for abrupt and linearly graded junctions, respectively. The parameter g is obtained by plotting the natural logarithm of the junction capacitance versus the natural logarithm of the reverse voltage

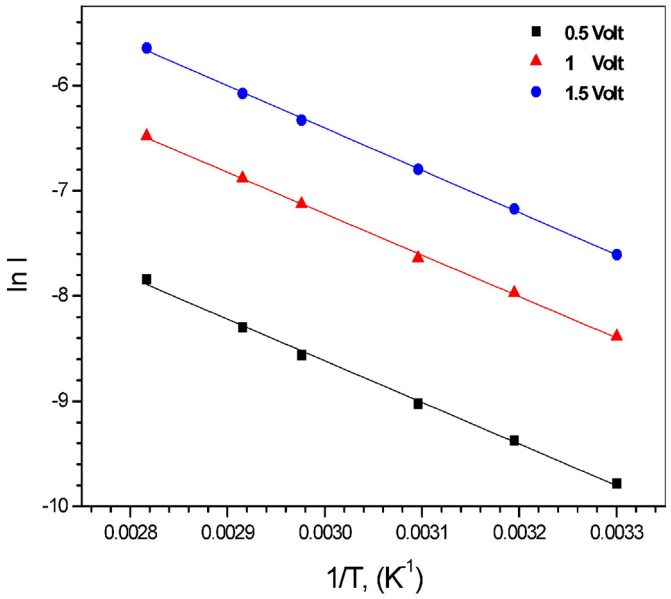

Fig. 6. Dependence of ln I on reciprocal temperature at different bias potentials.

(*g* is the slope of this curve). The obtained value of *g* is equal to 0.6 indicating that the junction is of abrupt nature.

Fig. 7 shows the ($C^{-2} - V$) characteristics at room temperature for Au/NR/p-Si/Al device measured in dark condition. For the abrupt heterojunction diode the relation between capacitance and bias potential [28] is:

$$\frac{1}{C^2} = -\frac{2(N_d\varepsilon_d + N_a\varepsilon_a)(V_b - V)}{e\varepsilon_d\varepsilon_a N_d N_a A^2} \tag{7}$$

where ε_d and ε_a are the permittivity of the donor and acceptor semiconductors, respectively, N_d and N_a are the carrier concentration of the ionized donor and acceptor atoms, A is the effective area of the device, V_b is the built-in potential and V is the applied voltage. From Fig. 7 it is clear that a plot of C^{-2} vs. V gives a straight line; from the intercept with the abscissa axis the value of built-in potential for the diode was calculated as 0.32 V, this value is comparable with the value of the barrier height predicted previously by thermionic emission model. The free carriers concentration, N, can be calculated from the slope of the straight line according to the relation [28]:

$$\text{Slope} = \frac{d\left(C^{-2}\right)}{dV} = -\frac{2}{e\varepsilon_r\varepsilon_o NA^2} \tag{8}$$

where N is the free carrier concentration. By using the permittivity of the NR ($\varepsilon_r\varepsilon_o = 2.7 \times 10^{-11}$ Fm^{-1}) [14] and the effective area of the device ($A = 0.12$ cm^2); the value of the free carriers concentration N was calculated as 4.5×10^{16} m^{-3}.

The barrier height can be determined as [29]:

$$\phi_b = V_b + V_n + \frac{K_B T}{q}, \tag{9}$$

$$V_n = \frac{K_B T}{q} \ln\left(\frac{N_v}{N}\right) \tag{10}$$

from these equations, barrier height, $\varphi_{b(C\text{-}V)}$, was found to be 0.49 eV. The barrier height obtained from (C–V) measurements, $\varphi_{b(C\text{-}V)}$ is higher than $\varphi_{b(I\text{-}V)} = 0.45$ eV derived from the (I–V) measurements. This discrepancy is probably due to barrier height inhomogeneity.

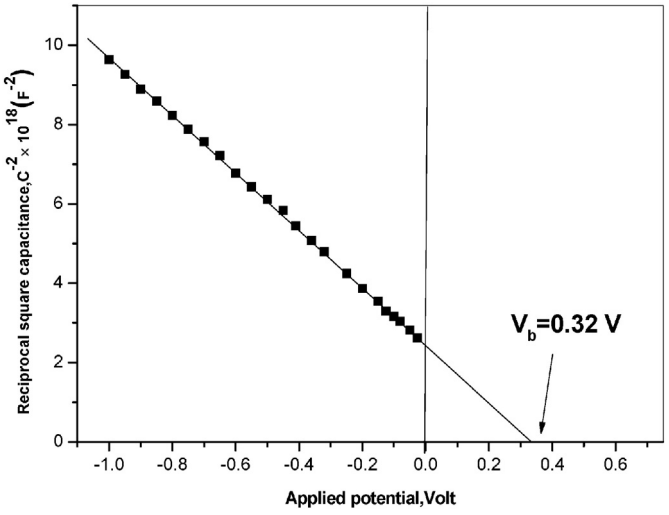

Fig. 7. Variation of C^{-2} with V of Au/p-NR/p-Si/Al heterojunction cell measured at room temperature in dark condition.

3.5. The energy band diagram of Au/NR/p-Si/Al heterojunction solar cell

Several studies based on donor–acceptor heterojunctions were performed to enhance the performance of the organic–inorganic photovoltaic devices. Silicon is a good candidate inorganic material for hybrid heterojunction devices due to strong absorption in UV–vis region, desirable electronic properties and the high dielectric constant compared to NR which prevents back transfer and improves transport of excitons through the interface. At interface between organic and inorganic materials, electrostatic forces result from the difference in affinity and ionization potential between the two different materials. The energy released when an electron is added to a gaseous atom which is in its ground state to form a gaseous negative ion is defined as the first electron affinity. The symbol is E_A and the unit is kJ/mol. The ionization energy, E_I, of an atom/ion is the minimum energy which is required to remove an electron of an atom. The unit of ionization energy is kJ/mol [30]. When both of electron affinity and ionization potential are greater in the silicon material than the NR material then the interfacial electric field derives charge separation as shown in Fig. 8.

If both LUMO and HOMO states of NR lie at energies sufficiently higher than those of the silicon, then the photogenerated exciton diffuses through the NR layer until it reaches to the donor–acceptor interface to dissociate and leave positive polaron on the NR and a negative polaron on the silicon. In the presence of efficient photocurrent generation or photogenerated exciton due to photon absorption, the charge separation should compete with the interfacial recombination and transfer to metal contacts.

The work function is the energy to excite electron from Fermi level to the vacuum level, it has a value of 4.97 eV for p-Si [20]. The built in voltage, V_{bi}, is due to the difference in work function of Si, φ_{Si}, and work function of NR, φ_{NR}, where $V_{bi} = \varphi_{Si} - \varphi_{NR} = 0.49$ eV. Then,

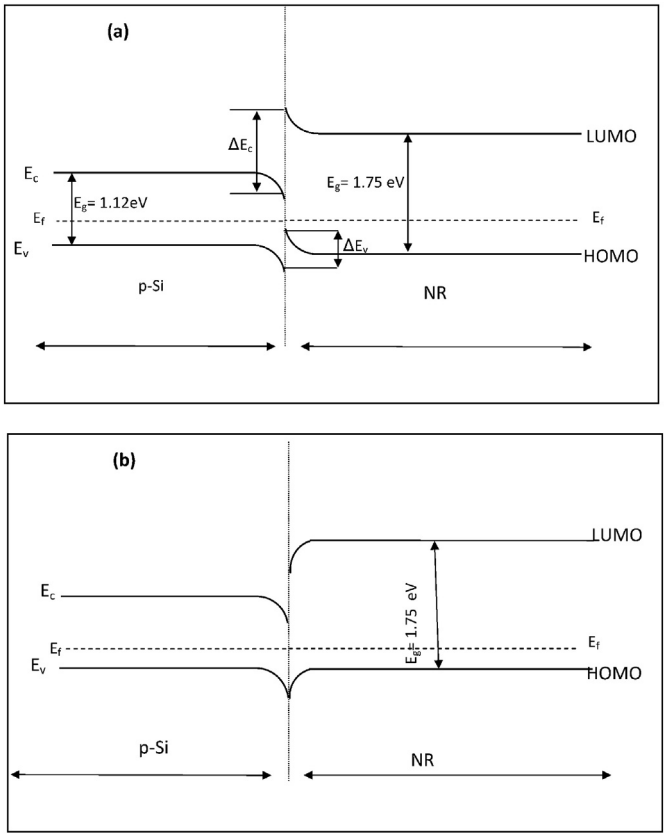

Fig. 8. Energy band diagram for NR/p-Si hybrid heterojunction device (a) For forward bias smaller than energy gap and (b) Modified profile due to the presence of charged interface.

$\varphi_{NR} = 4.48$ eV. When two different semiconductors fused together to form heterojunction diode, discontinuities form in the energy bands due to Fermi level alignment, these discontinuities in the conduction band, ΔE_c, are equal to the difference in electron affinities of two semiconductors [31]

$$\Delta E_c = \chi_{si} - \chi_{NR} \tag{11}$$

where χ_{si} and χ_{NR} are electron affinities of Si and NR, respectively, while the discontinuities in the valence band in the band gap, $\Delta E_{v,}$ is given by.

$$\Delta E_v = \Delta E_g - \Delta E_c \tag{12}$$

where ΔE_g is the difference in the band gap of two semiconductors. The band gap of Si 1.12 eV [26] and that of NR is 1.75 eV [14]. Therefore the energy band profile of that heterojunction can be constructed as shown in Fig. 8(a). For that heterojunctions ($\varphi_{Si} > \varphi_{NR}$), holes are depleted on the side containing the semiconductor with φ_{NR}, and are accumulated on the side containing the semiconductor with $\varphi_{Si,}$ this is referred to as a hole-accumulation/depletion heterojunction. The space charge region in Si layer consists of mobile electron charges, and the band was bent downwards from the bulk to interface, while in the NR layer, the band was bent upwards which causes an accumulation of holes near the interface and the energy band diagram in this case became as shown in Fig. 8(b).

3.6. I–V characteristics of the Au/NR /p-Si/Al heterojunction cell under illumination

Fig. 9 shows the power curve of the Au/NR/p-Si/Al heterojunction cell under illumination condition. The current value at a given voltage for this device under illumination is higher than in the dark (Fig. 3); this indicates that the absorption of light by the active layer generates excitons which dissociates into free-charge carriers at NR/Si interface resulting in the increase of photocurrent. This behavior yields useful information on the electron/hole pairs, which were effectively generated in the junction by incident photons. Under the influence of the electric field at the junction, the free electrons and holes were accelerated towards the electrodes along the potential barrier at the interface. As it is observed from Fig. 9, the device shows photovoltaic characteristics with open circuit voltage ($V_{oc} = 0.46$ V) , short circuit current ($I_{sc} = 1.78$ mA), voltage at maximum power point ($V_M = 0.25$ V) and current at maximum power point ($I_M = 0.95$ mA). The fill factor, *FF*, and the power conversion efficiency, η, of the heterojunction device are given by [19,32]:

$$FF = \frac{V_M I_M}{V_{oc} I_{sc}}, \tag{13}$$

and

$$\eta = \frac{V_{oc} I_{sc}}{A P_{in}} FF \times 100\% \tag{14}$$

where I_M and V_M are the current and voltage at maximum power point respectively, and P_{in} is illumination intensity impinging on the cell and A is the effective area. The values of fill factor and power conversion efficiency of the cell are 0.29 and 2.37%; respectively. The efficiency had been calculated without correcting for reflection or electrode absorption losses. Finally, the desirable feature of devices based NR supports this compound for the application in the photovoltaic solar cells and microelectronic devices. The results shown in Table 1 indicate that the efficiency of a solar cell depends on the type of organic compound used for light harvesting. The NR organic semiconductor compound satisfies the conditions imposed by Forrest et al. [40] on a particular organic molecule to form a high-quality rectifying contact barrier diode when deposited on an inorganic semiconductor substrate.

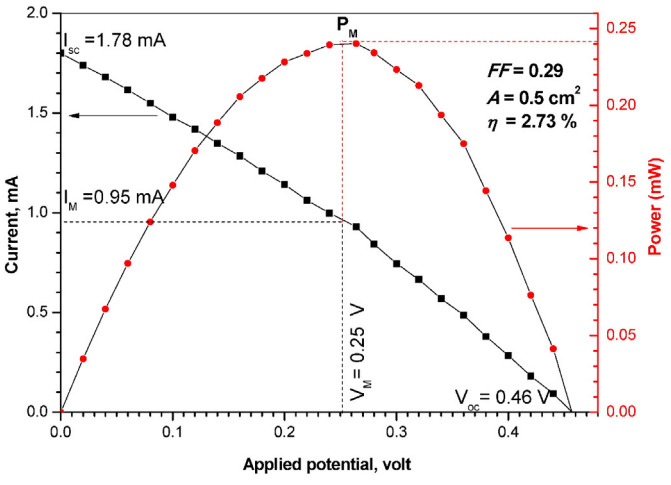

Fig. 9. (I–V) characteristic curve of maximum power region under illumination condition for Au/p-NR/p-Si/Al heterojunction solar cell measured at room temperature.

4. Conclusions

In the present work, neutral red (NR) thin films were grown on different substrates (glass, quartz and p-silicon) by thermal evaporation technique. The structure of NR films performed by using XRD patterns gave evidence for the nanocrystallites dispersed in amorphous matrix. The high absorption spectrum of NR films in visible region of spectra supports the application of NR film as an absorber in photovoltaic devices.

Hybrid Au/NR/p-Si/Al heterojunction device was fabricated and showed a series resistance of 2.64 kΩ, a shunt resistance of 237 kΩ, rectification ratio of 106 at ± 1 V and ideality factor of 1.8 at room temperature. At low voltages ≤0.2 V, the current in the device follows the thermionic emission model. In the voltage range $0.2 < V \leq 2$, the dominant conduction mechanism is a space-charge-limited current (SCLC) with a single trap level. Energy band diagram for NR/p-Si device was constructed and referred to a hole-accumulation/depletion heterojunction. The capacitance–voltage characteristics of the device were performed at room temperature in dark condition and the diode parameters such as built-in potential and carrier concentration were obtained as 0.32 V and 4.5×10^{16} m^{-3}, respectively.

The device under illumination with light of intensity 20 mW/cm^2 gives values of photovoltaic parameters as: 0.46 V, 1.78 mA, 0.29 and 2.73% for the open circuit voltage (V_{oc}), short circuit current (I_{sc}), fill factor (*FF*) and power conversion efficiency (η), respectively.

Table 1
Photovoltaic parameters of organic/inorganic solar cells based on different organic dyes and p-Si substrates.

Solar cell construction	J_{sc} (mA/cm^2)	V_{oc} (volt)	Fill factor (FF)	Efficiency (η %)	Ref.
Au/neutral red/p-Si/Al	3.56	0.46	0.29	2.73	Present work
Au/AlPcCl/p-Si/Al	0.043	0.22	0.72	2.60	[33]
Au/Perylene-66/p-Si/Al	0.003	0.07	0.20	–	[34]
Au/InPcCl/p-Si/Al	7.6	0.35	0.31	2.96	[35]
Au/TPP/p-Si/Al	6.2	0.5	0.35	2.13	[36]
Au/Methyl orange/p-Si/Al	14.9	0.37	0.31	–	[37]
Au/PTCDA/p-Si/Al	0.06	0.56	0.47	–	[38]
Au/PYR(G)/p-Si/Al	0.72	0.5	0.41	1.44	[39]

References

[1] R.W. Sabnis, Handbook of Acid–Base Indicators, CRC Press, Boca Raton, 2008 260.
[2] S. Kumar, K.R.J. Thomas, C.T. Li, K.C. Ho, Org. Electron. 26 (2015) 109.
[3] Hui Qi Zhang, William B. Euler, Sensors Actuators B Chem 225 (2016) 553.
[4] M. Hosseinnezhad, S. Moradian, K. Gharanjig, Dyes Pigments 123 (2015) 147.
[5] V. Sugathan, E. John, K. Sudhakar, Renew. Sust. Energ. Rev. 52 (2015) 54.
[6] M. Çakar, Y. Onganer, A. Türüt, Synth. Met. 126 (2002) 213.
[7] M.E. Aydın, T. Kılıçoğlu, K. Akkılıç, H. Hoşgören, Physica B 381 (2006) 113.
[8] K. Akkılıç, M.E. Aydın, İ. Uzun, T. Kılıçoğlu, Synth. Met. 156 (2006) 958.
[9] M.E. Aydın, F. Yakuphanoglu, J.H. Eomc, D.H. Hwang, Physica B 387 (2006) 239.
[10] R.W. Sabnis, Handbook of Biological Dyes and Stains: Synthesis and Industrial Applications, John Wiley and Sons, 2010.
[11] J. Fernando, W.S. Morgan, J.W. Hausser, J. Org. Chem. 32 (1967) 1120.
[12] Y. Ito, Chem. Abstr. 148 (2008) 264385.
[13] X. Zhang, F. Zhuanli, Chem. Abstr. 143 (2005) 356252.
[14] H.M. Zeyada, M.M. EL-Nahass, M.M. EL-Shabaan, J. Mater. Sci. 47 (2012) 493.
[15] E. Pinotti, A. Sassella, A. Borghesi, R. Paolesse, Synth. Met. 138 (2003) 15.
[16] R. Shirley, the CRYSFIRE System for Automatic Powder Indexing: User's Manual, The Lattice Press, Guildford, Surrey GU2 7NL, UK, 2000.
[17] J. Laugier, B. Bochu, LMGP-Suite of Programs for the interpretation of x-ray experiments, ENSP/Laboratoire des Materiaux et du Genie Physique, BP46.38042, Saint Martin d'Heres, France, 2000.
[18] M.M. Makhlouf, H.M. Zeyada, Synth. Met. 211 (2016) 1.
[19] S. Velumani, X. Mathew, P.J. Sebastian, Sol. Energy Mater. Sol. Cells 76 (2003) 359.
[20] H.M. Zeyada, M.M. EL-Nahass, M.M. Makhouf, Curr. Appl. Phys. 11 (2011) 1326.
[21] Y. Aydogdu, F. Yakuphanoglu, A. Aydogdu, M. Sekerci, Y. Balci, I. Aksoy, Synth. Met. 107 (1999) 191.
[22] M.M. El-Nahass, H.M. Zeyada, M.S. Aziz, M.M. Makhlouf, Thin Solid Films 492 (2005) 290.
[23] M.M. El-Nahass, K.F. Abd-El-Rahman, A.A.A. Darwish, Microelectron. J. 38 (2007) 91.
[24] S. Karatas, C. Temirci, M. Çakar, A. Türüt, Appl. Surf. Sci. 252 (2006) 2209.
[25] S.M. Sze, Physics of Semiconductor Devices, Wiley, New York, 1981 p. 97.
[26] E.H. Rhoderick, R.H. Williams, Metal–Semiconductor Contacts, Clarendon, Oxford, 1998 77.
[27] R.K. Gupta, R.A. Singh, J. Non-Cryst. Solids 351 (2005) 2022.
[28] M.S. Roy, G.D. Sharma, S.K. Gupta, Thin Solid Films 310 (1997) 279.
[29] M.A. Lampert, Rep. Prog. Phys. 27 (1964) 329.
[30] D.F. Shriver, P.W. Atkins, Shriver & Atkins' Inorganic Chemistry, 3th ed. Oxford University Press, Oxford, 1999.
[31] K. Nakayama, Y. Hashimoto, H. Sasabe, Y.J. Pu, M. Yokoyama, J. Kido, Jpn. J. Appl. Phys. 49 (2010) 01AB11.
[32] A.A.M. Farag, E.A.A. El-Shazly, M. Abdel Rafea, A. Ibrahim, Sol. Energy Mater. Sol. Cells 93 (2009) 1853.
[33] I.M. Soliman, M.M. El-Nahass, B.A. Khalifa, Synth. Met. 209 (2015) 55.
[34] M.M. El-Nahass, A.A.M. Farag, N.M. Khosifan, E.F.M. El-Zaidia, Synth. Met. 209 (2015) 74.
[35] H.M. Zeyada, M.M. El-Nahass, E.M. EL-Menyawey, A.S. EL-Sawah, Synth. Met. 207 (2015) 46.
[36] M.M. Makhlouf, H.M. Zeyada, Solid State Electron. 105 (2015) 51.
[37] A.A.M. Farag, A.M. Mansour, A.H. Ammar, M. Abdel Rafea, Synth. Met. 161 (2011) 2135.
[38] A.A.M. Farag, M. Fadel, Opt. Laser Technol. 45 (2013) 356.
[39] A.A.M. Farag, H.S. Soliman, A.A. Atta, Synth. Met. 161 (2012) 2759.
[40] S.R. Forrest, M.L. Kaplan, P.M. Schmidt, J. Appl. Phys. 56 (1984) 543.